THE JOURNAL OF BIOLOGICAL CHEMISTRY VOL. 288, NO. 31, pp. 22219–22232, August 2, 2013
Published in the U.S.A.

A TRPC1 Protein-dependent Pathway Regulates Osteoclast Formation and Function*[S]

Received for publication, February 6, 2013, and in revised form, May 24, 2013 Published, JBC Papers in Press, June 14, 2013, DOI 10.1074/jbc.M113.459826

E-Ching Ong[‡1,2], Vasyl Nesin[‡1], Courtney L. Long[§], Chang-Xi Bai[‡3], Jan L. Guz[‡], Ivaylo P. Ivanov[¶‖], Joel Abramowitz[**], Lutz Birnbaumer[**], Mary Beth Humphrey[§‡‡], and Leonidas Tsiokas[‡4]

From the Departments of [‡]Cell Biology and [§]Medicine/Rheumatology, University of Oklahoma Health Sciences Center, Oklahoma City, Oklahoma 73014, the [¶]BioSciences Institute, University College Cork, Cork, Ireland, the [‖]Department of Human Genetics, University of Utah, Salt Lake City, Utah 84112-5330, the [**]Laboratory of Neurobiology, Division of Intramural Research, NIEHS, National Institutes of Health, Department of Health and Human Services, Research Triangle Park, North Carolina 27709, and the [‡‡]Veterans Affairs Medical Center, Oklahoma City, Oklahoma 73014

Background: Ca^{2+} signaling is essential for osteoclastogenesis.
Results: I-mfa negatively regulates TRPC1-mediated Ca^{2+} signaling and osteoclastogenesis.
Conclusion: TRPC1 and I-mfa fine-tune the dynamic range of store-operated Ca^{2+} entry channels during osteoclastogenesis.
Significance: The TRPC1/I-mfa interaction is biologically relevant in osteoclastogenesis.

Ca^{2+} signaling is essential for bone homeostasis and skeletal development. Here, we show that the transient receptor potential canonical 1 (TRPC1) channel and the inhibitor of MyoD family, I-mfa, function antagonistically in the regulation of osteoclastogenesis. I-mfa null mice have an osteopenic phenotype characterized by increased osteoclast numbers and surface, which are normalized in mice lacking both *Trpc1* and *I-mfa*. *In vitro* differentiation of pre-osteoclasts derived from I-mfa-deficient mice leads to an increased number of mature osteoclasts and higher bone resorption per osteoclast. These parameters return to normal levels in osteoclasts derived from double mutant mice. Consistently, whole cell currents activated in response to the depletion of intracellular Ca^{2+} stores are larger in pre-osteoclasts derived from *I-mfa* knock-out mice compared with currents in wild type mice and normalized in cells derived from double mutant mice, suggesting a cell-autonomous effect of I-mfa on TRPC1 in these cells. A new splice variant of TRPC1 (TRPC1ϵ) was identified in early pre-osteoclasts. Heterologous expression of TRPC1ϵ in HEK293 cells revealed that it is unique among all known TRPC1 isoforms in its ability to amplify the activity of the Ca^{2+} release-activated Ca^{2+} (CRAC) channel, mediating store-operated currents. TRPC1ϵ physically interacts with Orai1, the pore-forming subunit of the CRAC channel, and I-mfa is recruited to the TRPC1ϵ-Orai1 complex through TRPC1ϵ suppressing CRAC channel activity. We propose that the positive and negative modulation of the CRAC channel by TRPC1ϵ and I-mfa, respectively, fine-tunes the dynamic range of the CRAC channel regulating osteoclastogenesis.

Mature osteoclasts are derived from hematopoietic stem cells through a series of events initiated by the formation of myeloid precursors in response to macrophage-colony stimulating factor (M-CSF)[5] (1). Subsequently, these precursors differentiate into multinucleated osteoclasts in a multistep process dependent on M-CSF and receptor activator of nuclear factor-κB ligand (RANKL) (2). Both of these factors act through Ca^{2+} signaling to induce downstream regulators of osteoclastogenesis such as nuclear factor of activated T cells c1 (NFATc1), NF-κB, c-*fos*, β-catenin, and others (3, 4). However, the molecular identity of the Ca^{2+} channels essential for osteoclastogenesis is only recently starting to emerge.

Store-operated Ca^{2+} entry (SOCE) channels, or Ca^{2+} channels activated in response to the depletion of intracellular Ca^{2+} stores, are thought to mediate Ca^{2+} signaling in early osteoclastogenesis (5), whereas transient receptor potential channels belonging to the vanilloid subgroup function at later stages of osteoclastogenesis (6–8). SOCE channels fall into two main types, the highly Ca^{2+}-selective Ca^{2+} release-activated Ca^{2+} (CRAC) channel (9) and the less Ca^{2+}-selective store-operated Ca^{2+} (SOC) channel (10, 11). The CRAC channel current (I_{CRAC}) is produced by the concerted action of a core SOCE protein Orai (also known as CRACM) and endoplasmic reticulum (ER) sensors, stromal interacting molecules 1 and 2 (STIM1 and -2), (12–21). STIM1 and STIM2 are single-pass

* This work was supported, in whole or in part, by National Institutes of Health Intramural Research Program Project Z01 ES101684 from NIEHS (to L. B.), Grant DE019398NIDCR (to M. B. H.), Grant R01DK59599 from NIDDK, and Grants P20GM103639 and P20GM104934NIGMS (to L. T.). This work was also supported by the Oklahoma Center for Adult Stem Cells.
[S] This article contains supplemental Fig. S1.
[1] Both authors contributed equally to this work.
[2] Present address: Cardiovascular Biology Program, Oklahoma Medical Research Foundation, 825 NE, 13th St., Oklahoma City, OK 73104.
[3] Present address: School of Mongolian Medicine, Inner Mongolia Medical College, Hohhot 010110, Inner Mongolia, China.
[4] To whom correspondence should be addressed: Dept. of Cell Biology, University of Oklahoma Health Sciences Center, 975 NE 10th St., Oklahoma City, OK. Tel.: 405-271-8001 (Ext. 46211); Fax: 405-271-3748; E-mail: ltsiokas@ouhsc.edu.

[5] The abbreviations used are: M-CSF, macrophage-colony stimulating factor; TRPC1, transient receptor potential canonical 1; TRPC1α, TRPC1 isoform α; TRPC1ϵ, TRPC1 isoform ϵ; I-mfa, inhibitor of MyoD family; CRAC channel, Ca^{2+} release-activated Ca^{2+} channel; SOCE, store-operated Ca^{2+} entry; STIM1, stromal interacting molecule 1; RANKL, receptor activator of nuclear factor-κB ligand; μCT, micro-computed tomography; BAPTA, 1,2-bis(2-aminophenoxy)ethane-*N*,*N*,*N*′,*N*′-tetraacetic acid; SOC store-operated Ca^{2+}; ER, endoplasmic reticulum; Fwd, forward; Rev, reverse; DKO, double knock-out.

membrane proteins primarily localized in the ER (20, 22), whereas Orai proteins (Orai1, -2, and -3) are four-pass membrane proteins localized at the plasma membrane (17). In response to the depletion of ER Ca^{2+} stores, STIM1 forms oligomers and accumulates at sites where the ER membrane is in close proximity to the plasma membrane to activate Orai proteins (23–27). Activated Orai mediates I_{CRAC} (13, 28, 29).

The molecular makeup and mode of activation of the channels mediating I_{SOC} are less clear, but TRPC1 has been shown to produce I_{SOC} in association with STIM1 and Orai1 (30–38). However, TRPC1 alone or co-expressed with STIM1 and Orai1 has never resulted in the *de novo* generation or amplification of I_{CRAC}, respectively. These results raise the question of whether the SOC and CRAC channel is the same channel modified by the presence or absence of TRPC1. Therefore, the exact role of TRPC1 in the regulation of store-operated Ca^{2+} entry pathways has been unclear.

I-mfa is a cytosolic protein with a unique cysteine-rich domain, first identified as an interacting protein interacting with MyoD (39) and subsequently with components of the Wnt/β-catenin pathway (40–43). We have identified the inhibitor of MyoD family isoform "a" (I-mfa) as a binding partner for TRPC1 (44). Using an array of biochemical assays, we showed that TRPC1 associated directly with I-mfa in transfected cells, native tissues, and cell lines. Functional experiments in transfected and native A431 cells revealed that I-mfa suppressed I_{SOC} through TRPC1. These gain- and loss-of-function experiments in combination with co-immunoprecipitation experiments in native tissues provided evidence for a physiological role of I-mfa in the regulation of endogenous TRPC1 activity. However, the biological role of the I-mfa-mediated inhibition of TRPC1 remained unknown. In this study, we identify a role of the TRPC1/I-mfa interaction in the regulation of osteoclastogenesis *in vivo* and *in vitro* through the modulation of the store-operated Ca^{2+} entry channels.

EXPERIMENTAL PROCEDURES

Animals—Mice were maintained under pathogen-free conditions in the barrier facility of University of Oklahoma Health Sciences Center. All procedures were approved by the Institutional Care and Use Committee of University of Oklahoma Health Sciences Center. Wild type (*I-mfa*$^{+/+}$) and *I-mfa*$^{-/-}$ mice were on a 129/SvJaeSor background (45). Wild type (*Trpc1*$^{+/+}$) and *Trpc1*$^{-/-}$ mice were on a pure 129/SvEv background (46). To generate *I-mfa/TRPC1* double knock-out animals, we crossed *Trpc1*$^{+/-}$ (in 129/SvEv background) with *I-mfa*+/− (50:50%, 129SvEv/129SvJaeSor) to derive the following four strains of mice: *Trpc1*$^{+/+}$;*I-mfa*$^{+/+}$ (wild type, WT), *Trpc1*$^{-/-}$;*I-mfa*$^{+/+}$ (*C1*$^{-/-}$), *Trpc1*$^{+/+}$;*I-mfa*$^{-/-}$ (*I*$^{-/-}$), and *Trpc1*$^{-/-}$;*I-mfa*$^{-/-}$ (double knock-out, DKO). DKO mice required multiple generations after crossing the single heterozygous mice.

Cell Culture—HEK293 cells were purchased from American Type Culture Collection (ATCC) and maintained in Dulbecco's modified Eagle's medium (DMEM, Mediatech) supplemented with 10% fetal bovine serum (FBS).

Plasmids—cDNAs encoding human Orai1 in pCMV-SPORT6 (BC015369), mouse STIM1 in pCMV-SPORT6 (BC021644), or mouse TRPC1ϵ (CA327829) were obtained from Open Biosystems. TRPC1ϵ was subcloned from the pYX-Asc vector into pCDNA3. The coding sequence of TRPC1α corresponds to nucleotides 187–2901 of clone U73625; TRPC1ϵ corresponds to nucleotides 187–1152 and 1173–2901 of U73625; TRPC1α-ΔNTx contains nucleotides 472–2901 of U73625; and TRPC1ϵ-ΔNTx contains nucleotides 472–1152 and 1173–2901 of U73625.

Expression of I-mfa and TRPC1α/ϵ Isoforms in Pre-osteoclasts—Nonadherent bone marrow-derived cells from wild type mice were grown in α-minimal essential medium supplemented with 10% ES-FBS (Atlanta Biologicals), 1× penicillin/streptomycin/glutamine solution (Invitrogen), and in the presence of 10% CMG-conditioned media (containing M-CSF). For experiments without M-CSF, 10% CMG was omitted from culture media. After 2 days, cells in suspension were collected, and total RNA was isolated using TRIzol (Invitrogen). Five μg of RNA was reverse-transcribed using SuperScript III (Invitrogen) and an equal mix of oligo(dT) and random hexamers (Roche Applied Science) as primers. I-mfa mRNA was detected using the following PCR primers: Fwd 5′-AGC CAC GAC CAC CTC TCA GAA CCG-3′ and Rev 5′-CGC AGT CCA GGA GGA TGT TAC AGA-3′. TRPC1 product was amplified using a primer set spanning the exon 4–5 junction, Fwd 5′-GTT GTC AGT CCG CAG ATG CAC TTT-3′ and Rev 5′-TGT CCA AAC CAA ACC GTG TTC AGG-3′ (694 bp). PCR conditions were as follows: initial denaturation for 2 min at 95 °C, 35 cycles of 30 s at 95 °C, 30 s at 57 °C, 45 s at 72 °C, and a final extension at 72 °C for 7 min using Platinum Taq polymerase (Invitrogen). The product of this PCR was used as a template for a nested PCR using the internal primer set: Fwd 5′- ACG ATC ATC AAG ACC AAC CAT TG-3′ and Rev 5′-AGT CCT CGT TTG TCA AGA GGC TCA-3′ (495 bp). PCR conditions were as follows: initial denaturation for 4 min at 96 °C, 30 cycles of 1 min at 96 °C, 1 min at 55 °C, 30s at 72 °C, and a final extension at 72 °C for 5 min using Vent polymerase (New England Biolabs) in a 200-μl reaction volume. PCR products were phenol/chloroform-extracted and ethanol-precipitated. An equal amount of purified PCR products were digested with EcoRV (New England Biolabs) or left untreated, separated on a 2% agarose gel, and photographed. Digested PCR products were subjected to one more round of amplification, EcoRV digestion, and separation on an agarose gel to ensure complete digestion of the TRPC1α isoform. Final EcoRV-resistant 500-bp band was excised, purified (Qiagen), and sequenced.

Real Time Quantitative PCR—Using gene-specific primers, quantitative real time PCR was performed with RT2 Fast SYBR Green quantitative PCR master mix (SABioscience, Valencia, CA) and the CFX96 detection system (Bio-Rad). PCR conditions were as follows: initial denaturation at 95 °C for 10 min, 40 cycles of 15 s at 95 °C, and 1-min extension at 61 °C for GAPDH and I-mfa, 55 °C for TRPC1α. Primer sets for I-mfa and GAPDH were same as above for RT-PCR. The TRPC1α-specific primer set used for real time quantitative PCR was Fwd 5′-GGT TTC GTC TTG ATA TCT ATA G-3′ and Rev 5′-TCG TTT GTC AAG AGG CTC ATC-3′.

Micro-computed Tomography (μCT) Analysis—Twelve-week-old male mice were euthanized, and soft tissues were

removed. After fixation in 70% ethanol, proximal tibiae were scanned by using the Scanco vivaCT 40 μCT scanner (Scanco Medical, Bassersdorf, Switzerland) with a resolution size of 10 μm. Three-dimensional reconstruction and quantification of structural parameters were calculated using the manufacturer's software. Scanning of the trabecular bone in the tibia was initiated proximal to the growth plate, and a total of 120 consecutive 10-μm-thick sections were analyzed. Cortical bone was excluded from the analysis, and the segmentation values were set at 0.8/1/220 for all studies.

Bone Histology and Histomorphometry—Tibiae were cut in half, and the larger distal pieces were fixed in 4% paraformaldehyde for 24 h at room temperature and stored in 70% ethanol until sectioning. Longitudinal sections (5 μm thick) were cut at the 50% plane from methyl methacrylate-embedded blocks using a Leica 2265 microtome. Sections were stained with Goldner's Trichrome. For histomorphometry, a region of interest was selected that was exactly 250 μm distal to the growth plate and extended 1 mm downward (thereby avoiding the primary spongiosa) through the metaphysis of the tibia. Standard bone histomorphometry was performed by the methods of Parfitt *et al.* (47) using Bioquant Image Analysis software (R & M Biometrics, Nashville, TN). Four types of primary measurements were made: area, length (perimeter), distance, and number. Tissue volume, bone volume, bone surface, and osteoid surface were used to derive trabecular number and trabecular separation. Blind measurements were performed in all samples.

Ex Vivo Osteoclast Differentiation—Three 8–12-week-old animals were used per experiment. Femurs, tibiae, and humeri were isolated, and soft tissue was removed. The bone marrow cavity was flushed with phosphate-buffered saline (PBS), and cells were grown in α-minimal essential medium supplemented with 10% embryonic stem cell-qualified (ES)-FBS (Atlanta Biologicals), 10% conditioned media from granulosa cells (CMG) (containing M-CSF), and 1× penicillin/streptomycin/glutamine solution (Invitrogen). After 2 days, cells in suspension were seeded at 50,000 cells/well on a hydroxyapatite substrate (Corning Glass) or at 50,000–200,000 cells/well on a 96-well plate, depending on the assay, and differentiated osteoclasts in medium were supplemented with 20 ng/ml recombinant mouse M-CSF and 50 ng/ml recombinant mouse RANKL (Shenandoah Biotechnology) for a defined period. To view resorption pits, osteoclasts were removed with 10% bleach, and the most representative areas of pits left by the osteoclasts were photographed and quantified using Metamorph (Molecular Devices) software. Pit area per osteoclast was determined only from nonoverlapping pits (100 pits/animal strain/experiment) using 50,000 cells plated per well onto osteologic plates (Corning Glass). Osteoclast resorption was confirmed by plating 50,000 pre-osteoclasts on dentin (Immunodiagnostic Systems Ltd.) for 10 days in the presence of 20 ng/ml M-CSF and 50 ng/ml RANKL. Cells were removed with a cotton swab and pits stained with Mayers hematoxylin (Sigma). Osteoclast multinucleation was determined by tartrate-resistant acid phosphatase staining of fixed cells. Fixed cells also were permeabilized with 0.1% Triton X-100 for 5 min, blocked with 1% BSA for 20 min at room temperature, and stained with phalloidin-Texas red (1:300, Molecular Probes) for 30 min at room temperature to visualize actin rings.

Transient Transfections—HEK293 cells were transfected in 35-mm dishes using Lipofectamine 2000 (Invitrogen) with the following plasmids: 1 μg of Orai1, 1.6 μg of STIM1, 1 μg of TRPC1, 0.3 μg of I-mfa or I-mfb, and 0.1 μg of CD8α. Cells were allowed to recover for 24 h, and then $CD8\alpha^+$ cells were identified by binding to magnetic beads coated with α-CD8α (Dynabeads®, DYNAL) and processed for electrophysiology.

Electrophysiology—Whole cell patch clamp experiments were performed in voltage clamp tight-seal configuration at room temperature. Recordings were acquired using the Warner PC-505B amplifier (Warner Instrument Corp., Hamden, CT) and pClamp9.2 software (Axon Instrument, Foster City, CA). Pipettes were pulled from borosilicate glass capillaries (Warner Instruments, Corp.) and polished to a final resistance of 2–4 megohms. Voltage ramps of 100 ms duration spanning a range of −100 to +100 mV were delivered from a holding potential of 0 mV at a rate of 0.5 Hz with an inter-ramp interval of 10 s. Currents were filtered at 2 kHz and digitized at 100-μs intervals. Capacitive currents were determined and corrected before each voltage ramp. Traces recorded before I_{CRAC} or I_{SOC} current activation were used as templates for leak subtraction. Standard external solution (bath) was as follows (in mM): NaCl 120, KCl 2.8, CsCl 10, $MgCl_2$ 2, $CaCl_2$ 10, HEPES 10, and glucose 10 at pH 7.2 with 300 mOsm NaOH. In HEK293 cells, 10 mM tetraethylammonium was added to suppress delayed rectifier-mediated K^+ currents (13). The standard internal solution (pipette) was as follow (in mM): cesium-methanesulfonate 120, NaCl 8, BAPTA 10, $MgCl_2$ 3, HEPES 10 at pH 7.2 with 300 mOsm CsOH. Extracellular Na^+ was replaced with an equimolar concentration of *N*-methyl-D-glucamine (Fig. 5*F*). Divalent replacement solution was based on the standard external solution, but 10 mM $CaCl_2$ was replaced by 10 mM $BaCl_2$. Whole cell currents in myeloid precursors were measured as described above in transfected cells, except for the concentration of $MgCl_2$ in the pipette solution, which was raised from 3 to 8 mM, to block possible contamination from endogenous TRPM7 currents.

Statistical Analysis—One-way analysis of variance followed by Newman-Keuls or Tukey-Kramer multiple comparisons post-test was used to determine statistical significance among measurements. *, $p < 0.05$; **, $p < 0.01$; ***, $p < 0.001$, and *ns* (nonsignificant), $p > 0.05$.

RESULTS

Trpc1 and I-mfa Function Antagonistically in the Regulation of Osteoclastogenesis—Despite mild skeletal patterning defects manifested as rib fusions and bifurcations and a mild form of spina bifida, *I-mfa*$^{-/-}$ mice are fertile and live to adulthood (45). *Trpc1*$^{-/-}$ mice also are fertile and live to adulthood (46). To test for a genetic interaction between the *Trpc1* and *I-mfa* genes, we generated compound *Trpc1*$^{-/-}$;*I-mfa*$^{-/-}$ mice and analyzed long bone histology and structure by histomorphometry and μCT (Figs. 1 and 2).

Histomorphometry revealed that *I-mfa*$^{-/-}$ mice had a significant reduction (44%) in bone mass accompanied by an increase in the number of osteoclasts per bone surface and ero-

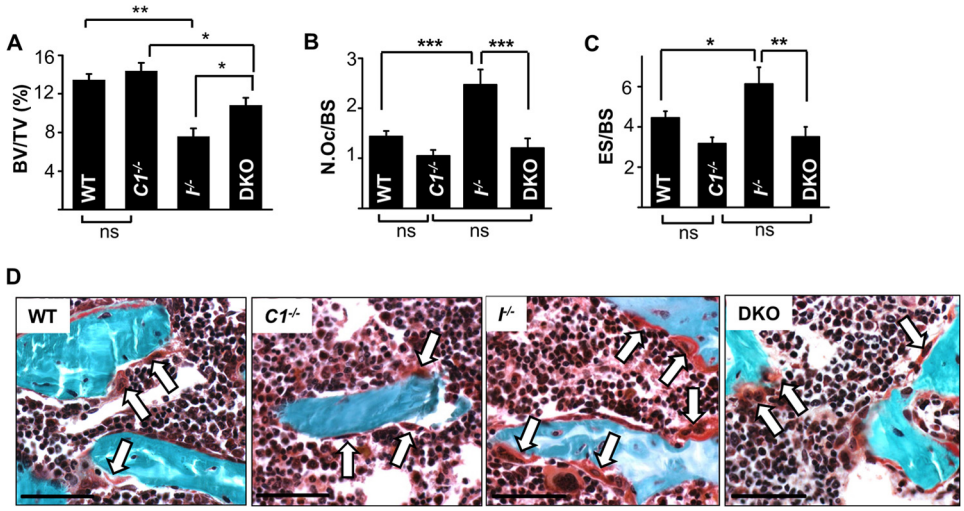

FIGURE 1. **Effects of single and double deletions of *Trpc1* and *I-mfa* genes on osteoclastogenesis *in vivo* determined by histomorphometry.** Summary data of bone volume/tissue volume (*BV/TV*) (*A*), osteoclast number/bone surface (*N.Oc/BS*) (*B*), or erosion (or osteoclast) surface/bone surface (*ES/BS*) (*C*) in tibiae of 12-week-old *Trpc1*$^{+/+}$;*I-mfa*$^{+/+}$ (WT, $n = 30$), *Trpc1*$^{-/-}$;*I-mfa*$^{+/+}$ (*C1*$^{-/-}$, $n = 18$), *Trpc1*$^{+/+}$;*I-mfa*$^{-/-}$ (*I*$^{-/-}$, $n = 18$), and *Trpc1*$^{-/-}$;*I-mfa*$^{-/-}$ (DKO, $n = 17$) male mice. Data were obtained by quantitative analysis of static histomorphometric indices using Goldner's Trichrome staining. Data represent mean ± S.E. *ns,* nonsignificant. *D,* representative images of Goldner's Trichrome stained sections of tibiae of four indicated strains of mice. *Arrows* indicate osteoclasts. *Scale bar,* 50 μm.

sion (or osteoclast) surface per bone surface, by 72 and 38%, respectively, compared with wild type controls, indicating an osteopenic phenotype (Fig. 1, *A*–*D*). In contrast to *I-mfa*$^{-/-}$ mice, single *Trpc1*$^{-/-}$ mice showed a substantial, but not significant, increase of 14% in bone mass and decreases of 27 and 28% in osteoclast numbers and eroded surface, respectively (Fig. 1, *A*–*D*). The higher osteoclast numbers and larger erosion surface per bone surface in I-mfa null mice were normalized in the double knock-out mice (Fig. 1, *A*–*D*), suggesting that the increased osteoclastogenesis seen in *I-mfa* mutant mice was related to increased activity of TRPC1.

μCT analysis confirmed the histomorphometry results. *I-mfa*$^{-/-}$ mice had severely reduced bone mass (42% reduction, Fig. 1, *A* and *F*), trabecular thickness, numbers, and connectivity density and increased trabecular spacing (Fig. 2, *B*–*E*). In contrast, *Trpc1*-deficient mice had significantly increased bone mass (13%, Fig. 2*A*) and connectivity density (Fig. 2*E*), but all other parameters were similar to control mice (Fig. 2, *B*–*D*). Double mutant mice had an intermediate phenotype with ~25% rescue of the *I-mfa*$^{-/-}$-reduced bone phenotype in regard to bone mass and trabecular thickness (Fig. 2, *A* and *C*). All other parameters in these mice remained similar to I-mfa null mice (Fig. 2, *B*, *D*, and *E*).

To determine whether the changes in bone mass were due in part to abnormalities in osteoblast numbers or function, we performed dynamic bone labeling prior to histomorphometry. Numbers and surface of osteoblasts and dynamic bone formation determined by calcein labeling were not different between wild type, I-mfa-knock-out mice, and DKO mice (Fig. 3) indicating a specific effect of I-mfa on osteoclasts and the lack of a significant genetic interaction of *I-mfa* and *Trpc1* in osteoblasts. Interestingly, the numbers of osteoblasts (Fig. 3*A*), but not mineral apposition rate or bone formation rate (Fig. 3, *D* and *E*), were reduced in *Trpc1*-null mice suggesting that osteoblasts lacking *Trpc1* may have increased function to compensate for the reduced numbers. In sum, both histomorphometric and μCT studies showed that deletion of I-mfa caused an osteopenic phenotype that was partially rescued by the deletion of both genes. At the cellular level, *I-mfa* null mice had increased numbers of osteoclasts, which were completely restored by the additional deletion of *Trpc1*, suggesting a dominant effect of TRPC1 over I-mfa in osteoclastogenesis *in vivo*.

To determine whether the effect of I-mfa-mediated inhibition of TRPC1 could affect osteoclast function in a cell-autonomous fashion, we performed *ex vivo* experiments in which bone marrow pre-osteoclasts were differentiated into mature, multinucleated osteoclasts in the presence of M-CSF and RANKL (Fig. 4*A*). Osteoclast function was determined by the size of resorption pits formed by individual osteoclasts plated onto hydroxyapatite-coated plates (Fig. 4, *B* and *C*) or dentin discs (Fig. 4*G*). Deletion of *Trpc1* did not significantly affect osteoclast formation (Fig. 4*A*) or resorption (Fig. 4, *B* and *C*), consistent with the idea that TRPC1 is blocked by I-mfa in wild type cells. However, deletion of *I-mfa* increased osteoclast numbers and resorption (Fig. 4, *A*–*C*). Inactivation of both *Trpc1* and *I-mfa* normalized osteoclast numbers and resorption (Fig. 4, *A*–*C*), suggesting that the effect of I-mfa on osteoclast formation and function was primarily mediated through the inhibition of TRPC1. Deletion of *I-mfa* or both genes did not have a specific effect on small, medium, or large osteoclasts *ex vivo* or actin ring formation (Fig. 4, *D*–*F*). Overall, genetic experiments showed that disruption of *I-mfa* enhanced osteoclastogenesis *in vivo* and function *in vitro* and that both of these effects were suppressed by the additional disruption of *Trpc1*.

Expression of Trpc1 and I-mfa mRNAs in Early Osteoclast Progenitors and Identification of a New TRPC1 Isoform (TRPC1ϵ)—To begin investigating whether TRPC1 and I-mfa mediate their effects on osteoclastogenesis at an early essential step in this process, we examined expression of *I-mfa* and *Trpc1* mRNAs in hematopoietic progenitors (no M-CSF), myeloid precursors (+M-CSF, no RANKL), and early pre-osteoclasts

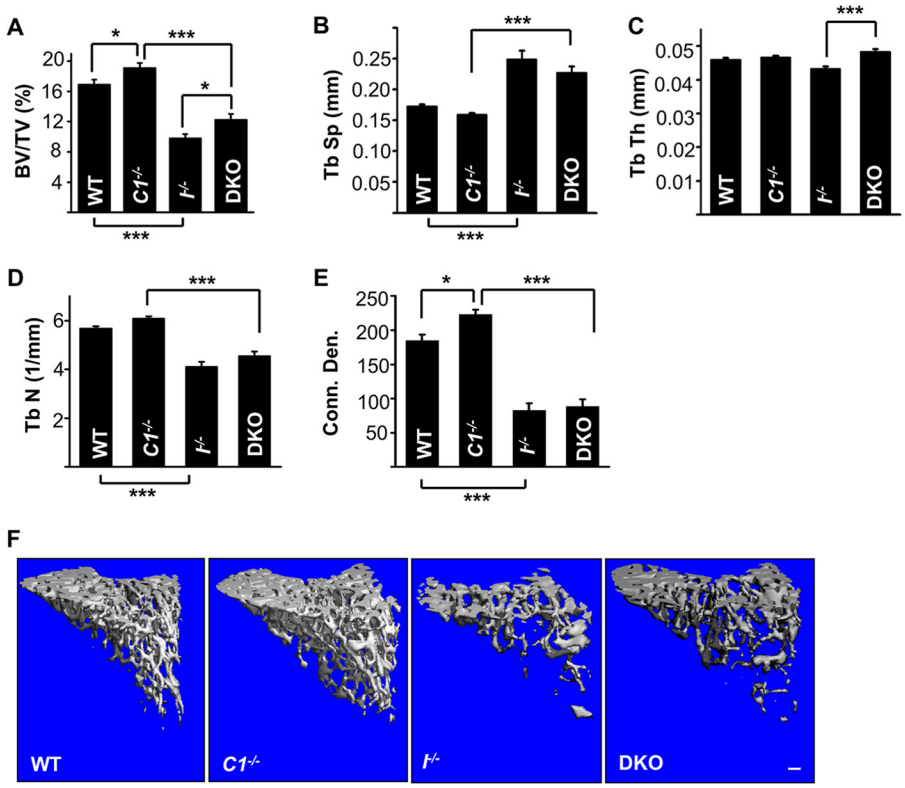

FIGURE 2. **Effects of single and double deletions of *Trpc1* and *I-mfa* genes on bone architecture determined by μCT.** Summary data of bone mass as indicated by bone volume/tissue volume (*BV/TV*) (*A*), trabecular spacing (*Tb Sp*) (*B*), trabecular thickness (*TbTh*) (*C*), trabecular number (*Tb N*) (*D*), or connectivity density (*Conn. Den*) (*E*) for all four mouse strains: $Trpc1^{+/+}$;$I\text{-}mfa^{+/+}$ (WT, $n = 12$), $Trpc1^{-/-}$;$I\text{-}mfa^{+/+}$ ($C1^{-/-}$, $n = 12$), $Trpc1^{+/+}$;$I\text{-}mfa^{-/-}$ ($I^{-/-}$, $n = 8$), and $Trpc1^{-/-}$;$I\text{-}mfa^{-/-}$ (DKO, $n = 17$). Data represent mean ± S.E. *F,* representative three-dimensional images of tibiae from the indicated strain of mice obtained by μCT. Analysis of tibia trabecular architecture was initiated proximal to the growth plate. *Scale bar,* 100 μm.

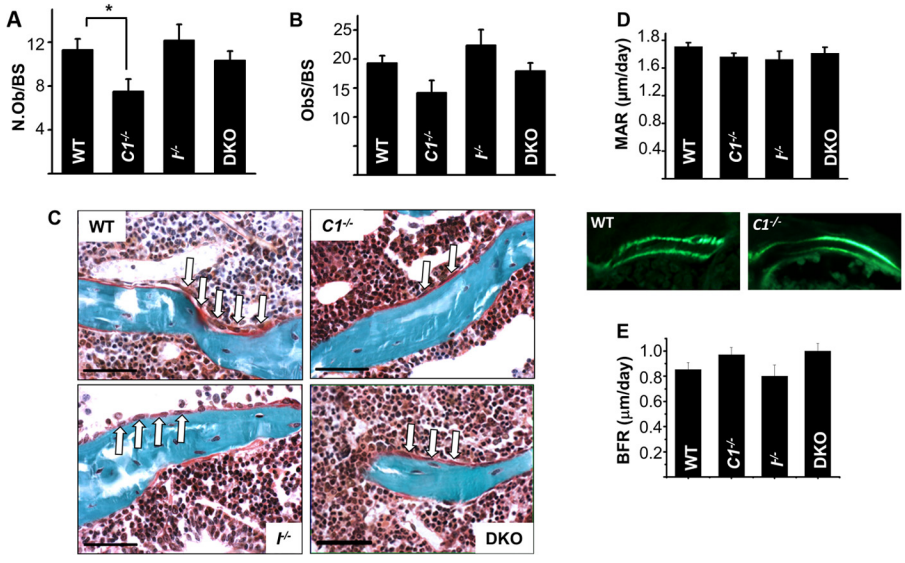

FIGURE 3. ***Trpc1* and *I-mfa* do not genetically interact to regulate osteoblast formation *in vivo*.** Osteoblast number/bone surface (*N.Ob/BS*) (*A*) and osteoblast surface per bone surface (*ObS/BS*) (*B*) in $Trpc1^{+/+}$;$I\text{-}mfa^{+/+}$ (WT, $n = 30$), $Trpc1^{-/-}$;$I\text{-}mfa^{+/+}$ ($C1^{-/-}$, $n = 18$), $Trpc1^{+/+}$;$I\text{-}mfa^{-/-}$ ($I^{-/-}$, $n = 18$), and $Trpc1^{-/-}$;$I\text{-}mfa^{-/-}$ (DKO, $n = 17$) from 12-week-old male mice were determined by bone histomorphometry. *C,* representative images of sections of the four indicated strains of mice. *Arrows* indicate osteoblasts. *Scale bar,* 25 μm. *D,* summary data and representative images of mineral apposition rate (*MAR*) (μm/day) determined by dynamic histomorphometry using double calcein labeling. *E,* bone formation rate (*BFR*) in μm per day. Data represent mean ± S.E.

(+M-CSF, +RANKL) (Fig. 5, *A–D*). *I-mfa* mRNA was induced by more than 20-fold during an early stage of differentiation in the presence M-CSF and then down-regulated in the later stage in the presence of M-CSF and RANKL. This regulation was consistent with its role as an inhibitor of Ca^{2+} signaling at an early stage in osteoclast differentiation (Fig. 5, *A* and *B*). Alternative splicing of the *Trpc1* gene results in several isoforms (α-δ) (48), with TRPC1α being the longest known isoform. RT-PCR showed expression of TRPC1α in hematopoietic progenitors and myeloid precursors that persisted in pre-osteoclasts

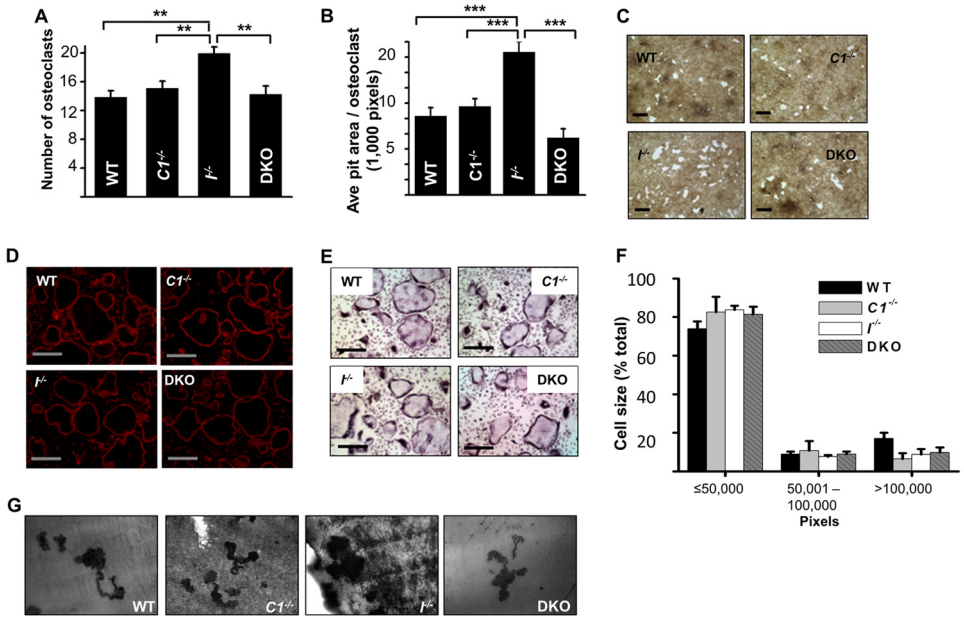

FIGURE 4. **Effects of single and double deletions of *Trpc1* and *I-mfa* genes on osteoclastogenesis *ex vivo*.** *A*, number of tartrate-resistant acid phosphatase-stained bone marrow-derived pre-osteoclasts cultured in the presence of 20 ng/ml recombinant M-CSF and 50 ng/ml RANKL for 4 days to visualize multinucleated osteoclasts. Cells with three or more nuclei were included in the analysis. Data in quadruplicates were obtained from four mice per group ($n = 4$). *Trpc1*$^{+/+}$;*I-mfa*$^{+/+}$ (WT), *Trpc1*$^{-/-}$;*I-mfa*$^{+/+}$ (*C1*$^{-/-}$), *Trpc1*$^{+/+}$;*I-mfa*$^{-/-}$ (*I*$^{-/-}$), and *Trpc1*$^{-/-}$;*I-mfa*$^{-/-}$ (DKO). *B*, average pit area in pixels from 100 nonoverlapping pits ($n = 100$) per each indicated genotype. Results from one out of two independent experiments are shown. In each experiment, 3–5 animals per genotype were used. *C*, representative images of resorption pits (*white*) left by mature and functional osteoclasts for each indicated genotype. *Scale bar*, 200 μm. *D*, representative images of phalloidin-Texas Red (1:300; Molecular Probes)-stained cells after 4 days in differentiation medium to visualize the formation of actin rings. *Scale bar*, 200 μm. *E*, representative images of tartrate-resistant acid phosphatase-stained multinucleated osteoclasts for each indicated genotype. *Scale bar*, 200 μm. *F*, size of multinucleated osteoclasts in all genotypes. Cells were classified as small (<50,000 pixels), medium (50,001–100,000 pixels), or large (>100,000 pixels) based on pixels per cell. Data represent mean ± S.E. *G*, *in vitro* derived osteoclasts effectively resorb dentin. 50,000 bone marrow-derived osteoclast precursors were plated on dentin discs in the presence of 50 ng/ml RANKL and 20 ng/ml MCSF for 10 days. Media were refreshed every 3 days. Cells were removed with a cotton swab and discs stained with Mayers hematoxylin to reveal the resorption pits (×20 magnification).

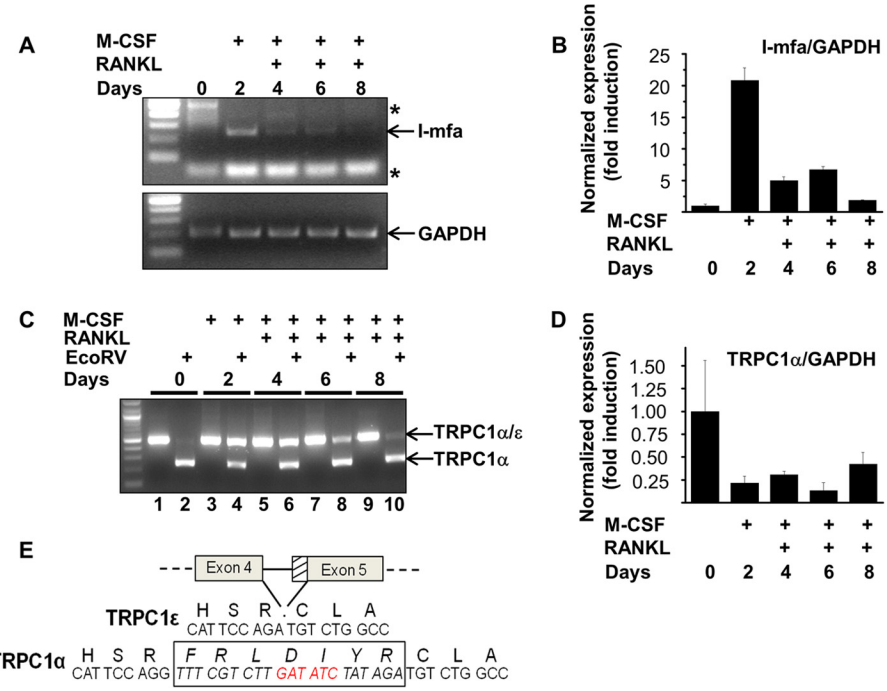

FIGURE 5. **Expression of I-mfa and TRPC1 in osteoclast precursors.** *A–D*, expression of *I-mfa or Trpc1* mRNA determined by RT-PCR (*A* and *C*) or real time quantitative PCR ($n = 3$) (*B* and *D*) in M-CSF-untreated (day 0) or M-CSF-treated (days 2, 4, 6, and 8) and RANKL-treated (days 4, 6, and 8) nonadherent freshly isolated bone marrow-derived cells. *Asterisk* indicates nonspecific band. *Trpc1* mRNA was reversed-transcribed, amplified by PCR, and digested with EcoRV. EcoRV-resistant PCR fragment at day 2 was gel-purified and directly sequenced. *Asterisks* indicate nonspecific products. *E*, nucleotide and corresponding amino acid sequence of the junction between exons 4 and 5 of mouse TRPC1α and TRPC1ϵ isoforms. Deleted sequence in TRPC1ϵ isoform is *boxed*. Unique EcoRV site in TRPC1α is shown in *red*.

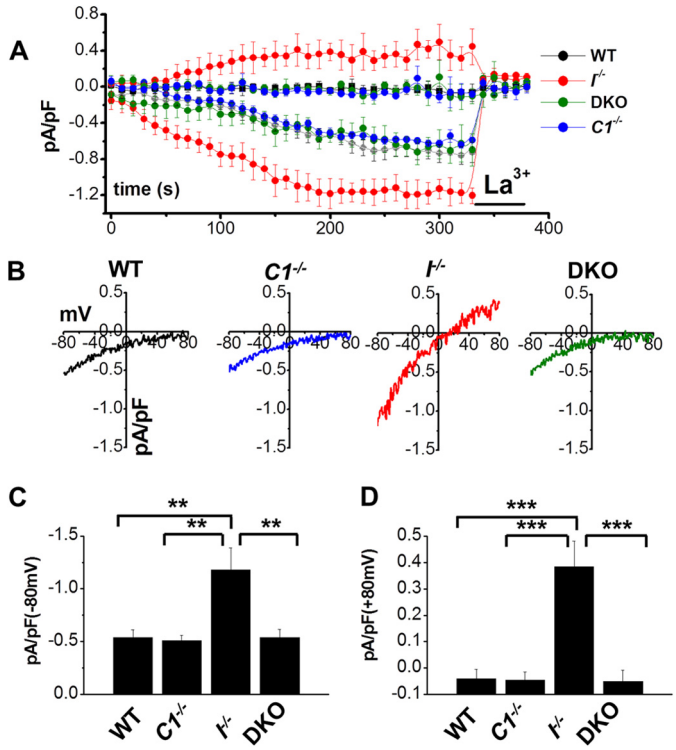

FIGURE 6. **Inhibition of TRPC1 by I-mfa in myeloid precursors.** *A,* time course of store-operated whole currents induced by 10 mM BAPTA in the recording pipette and inhibited by 20 μM La^{3+} applied in the extracellular solution in myeloid precursors (M-CSF-treated for 2 days) obtained from *Trpc1*$^{+/+}$;*I-mfa*$^{+/+}$ (WT, $n = 8$ cells), *Trpc1*$^{-/-}$;*I-mfa*$^{+/+}$ (*C1*$^{-/-}$, $n = 8$ cells), *Trpc1*$^{+/+}$;*I-mfa*$^{-/-}$ (*I*$^{-/-}$, $n = 12$ cells), and *Trpc1*$^{-/-}$;*I-mfa*$^{-/-}$ (DKO, $n = 9$ cells) mice. *B,* current-voltage (*I-V*) curve (taken at 200 s) of BAPTA-induced whole cell currents in cells derived from all four mouse strains. *C* and *D,* summary data of whole cell current density (*pA*/picofarads (*pF*)) at −80 (*C*) or +80 mV (*D*) of myeloid precursor cells derived from all four strains.

(Fig. 5*C*, *lanes 2, 4, 6, 8,* and *10*). Real time quantitative PCR however using 40 cycles, revealed down-regulation of TRPC1α in response to M-CSF by ~4–5-fold. However, due to very low expression level of TRPC1 in these cells and/or its expression in a subpopulation of these cells, quantitative changes in TRPC1 mRNA should be interpreted with caution. Interestingly, a new isoform (TRPC1ϵ) was induced in myeloid precursors in response to M-CSF and its expression persisted for 4 days following RANKL stimulation (Fig. 5*C*, EcoRV-resistant fragment in *lanes 2, 4, 6, 8,* and *10*). TRPC1ϵ differed from TRPC1α by the deletion of 21 nucleotides containing a unique EcoRV site that allowed us to efficiently distinguish the mRNAs of the two isoforms. The 21-nucleotide deletion, which was caused by an alternative use of a splice acceptor site residing 21 nucleotides downstream of the normal acceptor site at the beginning of exon 5 (Fig. 5*E*), resulted in an in-frame deletion of seven amino acids within the N-terminal cytosolic region (Fig. 5*E*).

Store-operated Whole Cell Currents in Myeloid Precursors—The expression of I-mfa and TRPC1 in myeloid precursors prompted us to examine store-operated currents in these cells. Cells derived from *Trpc1*$^{+/+}$;*I-mfa*$^{+/+}$ (WT) mice showed typical I_{CRAC} induced by 10 mM BAPTA in the pipette solution (Fig. 6, *A* and *B*, *black*). Deletion of *Trpc1* (*C1*$^{-/-}$ cells) did not affect I_{CRAC} (Fig. 6, *A* and *B*, *blue*), consistent with the idea that TRPC1 was blocked by I-mfa in these cells. However, deletion of *I-mfa* (*I*$^{-/-}$ cells) resulted in almost linear store-operated current(s) displaying a larger inward component than that of I_{CRAC} but also an outward component (Fig. 6, *A* and *B*, *red*). Currents in these cells were the largest among all groups (Fig. 6, *C* and *D*). Deletion of both genes (DKO cells) restored I_{CRAC} that was indistinguishable from I_{CRAC} seen in wild type or *Trpc1* null cells (Fig. 6, *A* and *B*, *green*), indicating that *Trpc1* was responsible for the formation of large linear currents(s). These data showed that endogenous TRPC1 augments store-operated currents and I-mfa suppresses the contribution of TRPC1 to these currents. Moreover, the effects of these two proteins on store-operated currents correlated well with their ability to modulate osteoclast formation and function, suggesting that modulation of store-operated currents by TRPC1 and I-mfa may underlie the mechanism of action of TRPC1 and I-mfa on osteoclastogenesis.

Translation of Trpc1 mRNA Is Initiated from a Non-AUG Codon—To obtain a mechanistic insight of how TRPC1 modulated these currents, we proceeded with a heterologous system whereby the two TRPC1 isoforms were functionally evaluated in HEK293 cells. However, we noticed that the 5′-untranslated region of mouse or human TRPC1α or TRPC1ϵ mRNA in exon 1 was extended far beyond the first methionine without an upstream in-frame STOP codon (Fig. 7*A* and supplemental Fig. S1). In fact, five putative non-AUG translation initiation sites, as predicted by Ivanov *et al.* (49), were identified upstream of the first methionine in 13 mammalian TRPC1 species (Fig. 7*A* and supplemental Fig. S1). To identify the most upstream functional non-AUG translational start site in TRPC1, we deleted or mutated sites 1–3 and tested for their effects on TRPC1 mobility in SDS-PAGE. Deletion of site 1 did not cause a significant change in TRPC1 size (Fig. 7, *B* and *C*, *lane 3*), suggesting that site 1 either was not utilized or it was utilized, but upon its deletion, translation was initiated at a nearby non-AUG site, possibly site 2. When site 2 was deleted along with site 1 (Fig. 7*C*, *lanes 4* and *5*) or singly mutated (Fig. 7*C*, *lane 6*), translation was initiated from a downstream site causing a reduction in TRPC1 size. This analysis suggested that site 2 functions as the most upstream non-AUG translational start site of mouse TRPC1 expressed in HEK293 cells (Fig. 7, *B* and *C*). To test whether translation of endogenous TRPC1 also is initiated upstream of the predicted AUG site, endogenous TRPC1 was immunoprecipitated from HEK293T cell lysates and detected with a monoclonal TRPC1-specific antibody (1F1) (Fig. 7*D*, *lane 5*). A TRPC1-specific band with a molecular size similar to TRPC1α/ϵ was detected (Fig. 7*D*, *lane 5*), arguing that endogenous TRPC1 contains a species with the N-terminal extension, as seen with transfected TRPC1 (Fig. 7*D*, *lane 2*). Overall, these data identify a new splice variant of TRPC1 induced in an early osteoclast precursor population by M-CSF and reveal that translation of transfected mouse or endogenous human TRPC1 is initiated at a CUG codon resulting in an N-terminal extension by 78 amino acids.

Functional Characterization of TRPC1α and TRPC1ϵ Isoforms—Functional expression of long (TRPC1α or TRPC1ϵ) or short TRPC1 isoforms without the N-terminal extension (TRPC1α-ΔNTx or TRPC1ϵ-ΔNTx) required co-expression with Orai1 and STIM1. TRPC1 overexpression alone did not

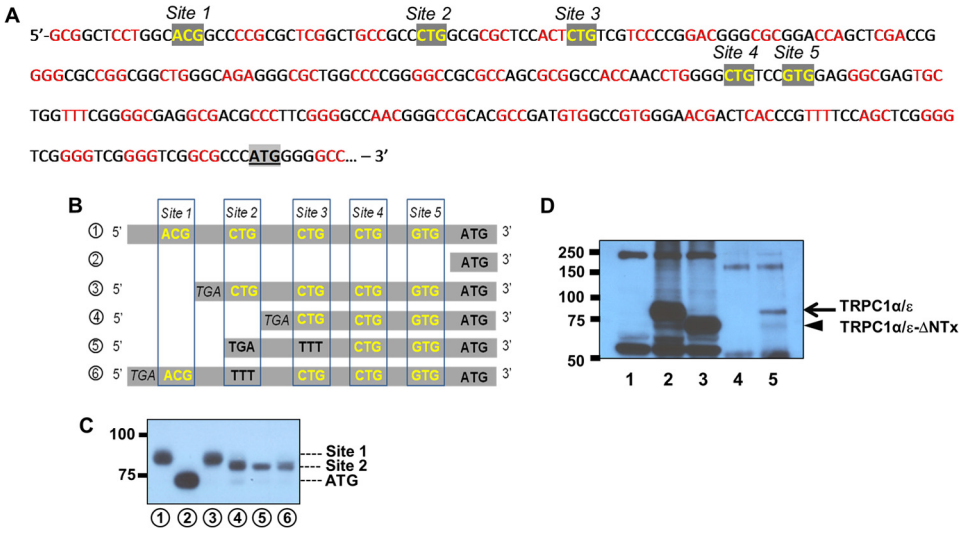

FIGURE 7. **Translation of TRPC1 is initiated from an upstream non-AUG site.** *A,* nucleotide sequence upstream of first AUG of mouse TRPC1. Potential non-AUG translation start sites (*Sites 1–5*) are *boxed*. *B,* predicted non-AUG translation start sites (*sites 1–5*) of mouse TRPC1 are *boxed*. *C,* mobility of TRPC1 constructs containing various lengths of the presumed 5′-untranslated region of mouse TRCP1α mRNA. HEK293T cell lysates transfected with the α-isoform of mouse TRPC1 cDNA containing the entire 5′-untranslated region (TRPC1α, *lane 1*), the α-isoform of mouse TRPC1α cDNA lacking the sequence upstream of the first predicted methionine (TRPC1α-ΔNTx, *lane 2*), TRPC1α cDNA lacking site 1 (*lane 3*), TRPC1α cDNA lacking sites 1 and 2 (*lane 4*), TRPC1α cDNA lacking sites 1–3 (*lane 5*), or TRPC1α cDNA with mutated site 2 (*lane 6*) were separated in 6% SDS-PAGE, immunoblotted, and probed with α-TRPC1 (1F1). *D,* translational initiation of endogenous human TRPC1 from a non-AUG site. HEK293T cell lysates transfected with pCDNA3 (mock-transfected, *lane 1*), TRPC1α (*lane 2*), or TRPC1α-ΔNTx (*lane 3*) were immunoblotted with α-TRPC1 (1F1). Endogenous TRPC1 was immunoprecipitated with mouse IgG (10 μg/ml lysates, negative control, *lane 4*) or 1F1 (10 μg/ml lysates, *lane 5*) and detected using 1F1.

produce any significant currents. Cells transfected with Orai1 + STIM1 + TRPC1α (OSTα) showed a large I_{SOC} (Fig. 8*A*). TRPC1α-ΔNTx also produced a large I_{SOC} when co-expressed with Orai1 and STIM1 (OSTα-ΔNTx) (Fig. 8*B*) but with a lower Ca^{2+} selectivity compared with TRPC1α, as whole cell currents in cells transfected with Orai1+ STIM1 + TRPC1α (OSTα) had a positive shift in the reversal potential (E_{rev}) by ~20 mV compared with cells transfected with Orai1 + STIM1 + TRPC1α-ΔNTx (OSTα-ΔNTx) (Fig. 8, *A* and *B*). These results indicated that the N-terminal extension modifies the ionic selectivity of Orai1, TRPC1α, or possibly TRPC1α/Orai1 channels.

Remarkably, co-expression of TRPC1ϵ with STIM1 and Orai1 did not produce I_{SOC} but instead amplified Orai1-mediated I_{CRAC} (Fig. 8*D*), as judged by activation by passive store depletion induced by BAPTA and formation of an inwardly rectifying current. Therefore, the 7-amino acid deletion generated by alternative splicing in TRPC1ϵ dramatically changed the permeability properties of TRPC1ϵ and/or Orai1/TRPC1ϵ complexes by completely eliminating the outward component in Orai1/TRPC1α-transfected cells, while enhancing inward currents in Orai1/TRPC1ϵ-transfected cells compared with Orai1-transfected cells.

Deletion of the N-terminal extension from TRPC1ϵ (TRPC1ϵ-ΔNTx) resulted in linear currents but with an E_{rev} closer to the E_{rev} of I_{SOC} in STIM1 + Orai1 + TRPC1α-transfected cells and some inward rectification (Fig. 8*C*). These data indicated that both the N-terminal extension and the 7-amino acid deletion were required for the amplification of Orai1-mediated currents by TRPC1ϵ, demonstrating for the first time that a transient receptor potential channel can amplify I_{CRAC} or a current closely resembling I_{CRAC}. Changes in STIM1 or Orai1 expression levels in cells transfected with or without TRPC1ϵ could not account for such an effect (Fig. 8*E*). Interestingly, overexpression of STIM1 and Orai1 in transiently transfected cells induced the expression of an endogenous TRPC1 species with a molecular size similar to TRPC1 constructs containing the N-terminal extension (Fig. 8*E*, *lanes 2, 4,* and *6*), supporting previous findings (Fig. 7*D*) that native human TRPC1 mRNA utilizes an upstream non-AUG site as seen in transfected mouse TRPC1. These data further reveal a possible regulation of TRPC1 protein by Orai1 and STIM1.

Next, we examined Ca^{2+} and Ba^{2+} permeability of Orai1 in the presence of TRPC1ϵ. Substitution of extracellular Na^+ with an equimolar concentration of the nonpermeable *N*-methyl-D-glucamine did not affect the size of store-operated inward currents in cells transfected with STIM1 + Orai1 or STIM1 + Orai1 +TRPC1ϵ suggesting that TRPC1ϵ amplified Orai1-mediated Ca^{2+} currents (Fig. 8*F*). However, TRPC1ϵ did increase the permeability of Orai1 to Ba^{2+}. Co-expression of TRPC1ϵ with STIM1 and Orai1 resulted in larger Ba^{2+} currents compared with STIM1 + Orai1 (Fig. 8*G*), strongly suggesting the formation of a heteromultimeric channel of Orai1 and TRPC1ϵ. As shown in Fig. 8*E*, expression levels of STIM1 and Orai1 were not affected by the presence or absence of TRPC1ϵ, which could potentially affect Ba^{2+} permeability in triple-transfected cells (50). Substitution of extracellular Ca^{2+} with a divalent-free solution proportionally augmented currents mediated by STIM1-activated Orai1 or Orai1/TRPC1ϵ, indicating that TRPC1ϵ did not affect monovalent permeability of STIM1-activated Orai1 channel (data not shown). Consistent with the qualitative rather than quantitative effects of TRPC1α and TRPC1ϵ on I_{CRAC}, both isoforms were expressed at comparable levels in the plasma membrane (Fig. 9, *middle panel, lanes 2* and *3*).

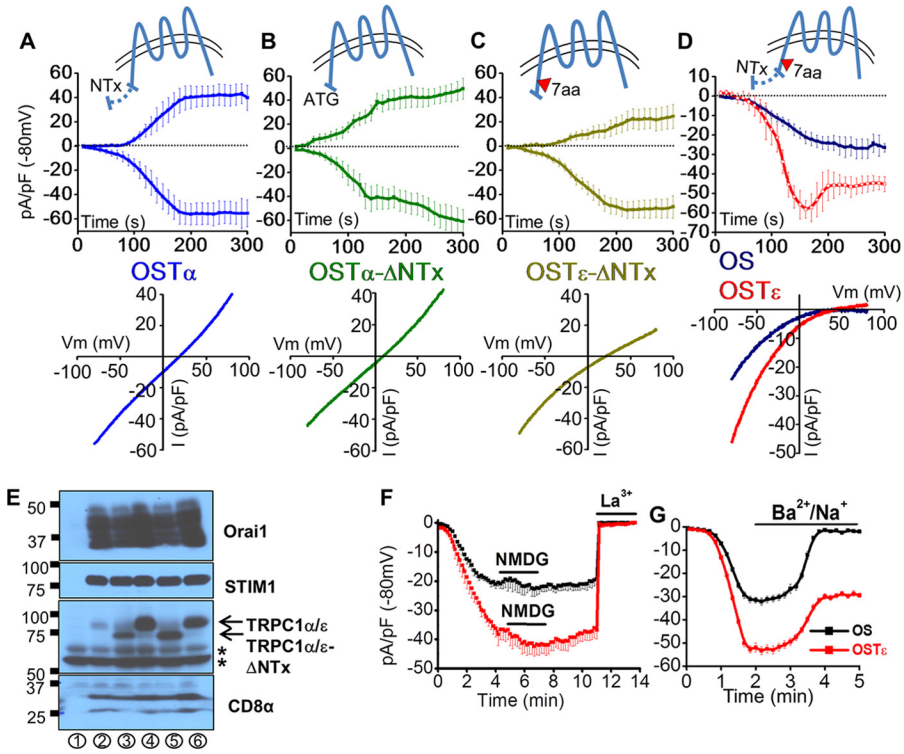

FIGURE 8. **Generation of I_{SOC} by TRPC1α and amplification of I_{CRAC} by TRPC1ϵ.** *A,* time course and *I–V* curve (taken at 200 s) of BAPTA-induced whole cell currents in cells transfected with STIM1 (1.6 μg), Orai1 (1 μg), and TRPC1α (1 μg), (n = 9). *pF*, picofarad. *B,* time course and *I–V* curve (taken at 200 s) of BAPTA-induced whole cell currents in cells transfected with STIM1 (1.6 μg), Orai1 (1 μg), and TRPC1α-ΔNTx (1 μg) (n = 10). *C,* time course and *I–V* curve (taken at 200 s) of BAPTA-induced whole cell currents in cells transfected with STIM1 (1.6 μg), Orai1 (1 μg), and TRPC1ϵ-ΔNTx (1 μg) (n = 14). *D,* time course and *I–V* curve (taken at 200 s) of BAPTA-induced whole cell currents in cells transfected with STIM1 (1.6 μg), Orai1 (1 μg), and TRPC1ϵ (1 μg) (*OSTϵ, red*, n = 11) or STIM1 (1.6 μg) and Orai1 (1 μg) (*OS*, *blue*, n = 8). *E,* expression levels of Orai1, STIM1, TRPC1, or CD8α in transfected HEK293T cells. Cell lysates transfected with GFP (negative control, *lane 1*), Orai1, STIM1, and CD8α (*lane 2*), Orai1, STIM1, TRPC1α-ΔNTx, and CD8α (*lane 3*), Orai1, STIM1, TRPC1α, and CD8α (*lane 4*), Orai1, STIM1, TRPC1ϵ-ΔNTx, and CD8α (*lane 5*), or Orai1, STIM1, TRPC1ϵ, and CD8α (*lane 6*) were immunoblotted with a rabbit polyclonal antibody to Orai1 (1:5000, Sigma), mouse monoclonal antibody to STIM1 (1:1000, Cell Signaling), mouse monoclonal to TRPC1 (1F1, 1:300), or rabbit polyclonal to CD8α (1:500, Santa Cruz Biotechnology). *Asterisks* indicate nonspecific bands. *F,* effects of Na^+ to *N*-methyl-D-glucamine substitution on whole cell currents induced by BAPTA (10 mM in pipette) in HEK293 cells transiently transfected with Orai1 and STIM1 (*OS*, *black*, (n = 5) or Orai1, STIM1, and TRPC1ϵ (*OSTϵ, red*, n = 8). *G,* effects of Ca^{2+} to Ba^{2+} substitution on whole cell currents induced by BAPTA (10 mM in pipette) in HEK293 cells transiently transfected with Orai1 and STIM1 (*OS*, *black*, n = 7) or Orai1, STIM1, and TRPC1ϵ (OSTϵ, *red*, n = 8).

Suppression of I_{SOC} and I_{CRAC} by I-mfa through TRPC1—Next, we tested the effect of I-mfa on I_{SOC} and I_{CRAC} in the presence or absence of TRPC1α or TRPC1ϵ, respectively. Fig. 10*A* shows that I-mfa suppressed I_{CRAC} in cells transfected with STIM1, Orai1, and TRPC1ϵ but not in cells transfected with STIM1 and Orai1. Expression levels of STIM1, Orai1, or TRPC1 did not change by co-transfection with I-mfa or I-mfb (Fig. 10*C*). I-mfb, which is a splice variant of I-mf lacking the TRPC1-binding site did not suppress I_{CRAC} (Fig. 10, *A* and *D*). Interestingly, I-mfa suppressed I_{CRAC} to a lower magnitude than the magnitude of I_{CRAC} mediated by Orai1 in the absence of TRPC1ϵ, suggesting that TRPC1ϵ "sensitized" Orai1 to I-mfa-mediated inhibition. I-mfa had a similar effect on I_{SOC} in cells transfected with STIM1, Orai1, and TRPC1α (Fig. 10, *B* and *D*). Because I-mfa does not physically interact with STIM1 or Orai1 (data not shown), does not disrupt the Orai1/TRPC1 interaction (Fig. 10*E*), and suppresses I_{SOC}/I_{CRAC} only in the presence of TRPC1α/ϵ (Fig. 10, *A* and *B*), we conclude that I-mfa suppresses these currents by being recruited to the Orai1-TRPC1 complex through an interaction with TRPC1α/ϵ. In sum, these results show that TRPC1 has a dual effect on Orai1-mediated I_{CRAC}. In the absence of I-mfa, TRPC1ϵ amplifies Orai1-mediated I_{CRAC}, whereas in the presence of I-mfa, it mediates I-mfa-induced inhibition of Orai1-mediated I_{CRAC}. The positive and negative modulation of Orai1-mediated current by TRPC1 and I-mfa, respectively, suggests that the dynamic range of the CRAC channel can be enhanced by TRPC1 and I-mfa.

DISCUSSION

Our study provides several lines of evidence supporting the hypothesis that *Trpc1* and *I-mfa* genetically and functionally interact to regulate osteoclastogenesis through store-operated Ca^{2+} entry channels. First, *I-mfa*$^{-/-}$ mice show increased osteoclast formation *in vivo*, which is suppressed in mice lacking both genes. Second, pre-osteoclasts derived from *I-mfa* null mice have an increased number of mature osteoclasts and higher resorptive activity per osteoclast, which are normalized in cells derived from double mutant mice. Third, store-operated Ca^{2+} currents are enhanced in I-mfa-null myeloid precursors and suppressed in double mutant cells. Fourth, TRPC1 requires core components of the CRAC channel, STIM1 and Orai1 for function, and I-mfa suppresses store-operated currents only in the presence of TRPC1. The data lead us to propose that TRPC1 and I-mfa increase the dynamic range of the

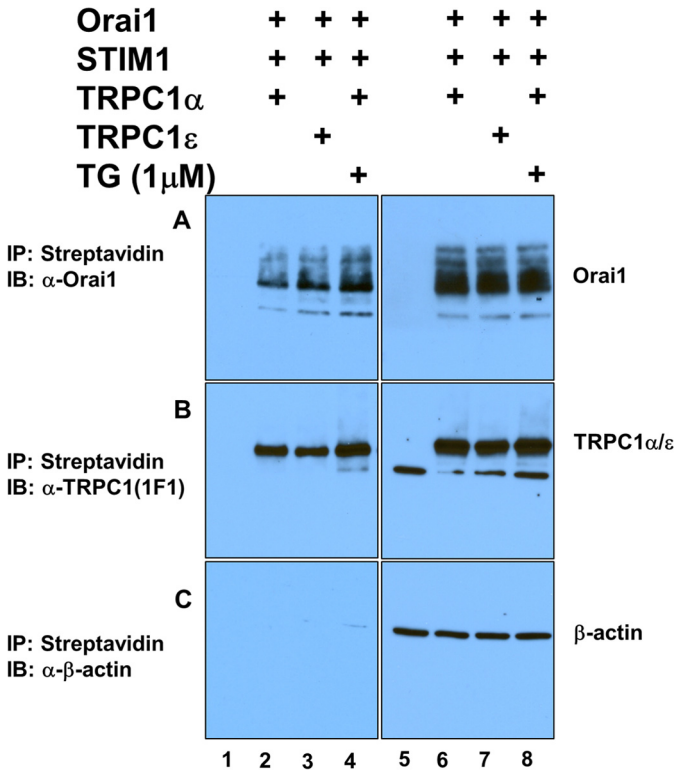

FIGURE 9. **Cell surface expression of TRPC1α and TRPC1ϵ in transiently transfected HEK293 cells.** Cells were left untrasfected (*lanes 1* and *5*) or transfected with STIM1 + Orai1 + TRPC1α (*lanes 2, 4, 6,* and *8*), or STIM1 + Orai1 + TRPC1ϵ (*lanes 3* and *7*) in 10-cm dishes using Lipofectamine 2000. Twenty four hours following transfection, cell surface proteins were biotinylated with 0.05 mg/ml cell impermeant biotin for 30 min at room temperature in PBS (pH 8.0), washed three times with PBS plus 100 mM glycine, and captured with streptavidin beads. Biotinylated proteins were probed with rabbit α-Orai1 (1:5000 dilution, Sigma) (*upper left panel*), mouse monoclonal α-TRPC1 (1F1, 3.4 μg/ml) (*middle left panel*), or mouse monoclonal α-β-actin (1:1000 dilution, Santa Cruz Biotechnology) (*lower left panel*). *Right panels* indicate input amounts of Orai1, TRPC1, and β-actin in lysates. Cells transfected with Orai1, STIM1, and TRPC1α were stimulated by 1 μM thapsigargin (*TG*) in DMEM supplemented with 10%FBS for 5 min before biotinylation (*lanes 4* and *8*). *IP*, immunoprecipitation; *IB*, immunoblot.

CRAC channel, which can account for the observed effects on osteoclastogenesis.

I-mfa null mice have a significant osteopenic phenotype with increased osteoclastogenesis. Because the effect of *I-mfa* deletion on osteoclastogenesis was completely rescued by the additional deletion of *Trpc1*, we suggest that I-mfa promoted osteoclastogenesis by a mechanism related to TRPC1 and unrelated to its role as an inhibitor of the MyoD and other basic helix-loop-helix transcription factors and/or through the canonical Wnt/β-catenin pathway. However, involvement of these pathways is likely to be important in regulating bone mass independently of osteoclastogenesis in I-mfa null mice. This is supported by the incomplete normalization of bone mass in compound mice compared with mice lacking I-mfa. In contrast to the osteoporosis of I-mfa null mice, TRPC1 null mice showed a mild increase in bone mass. The effect of the *Trpc1* deletion on osteoclastogenesis is revealed only in mice lacking I-mfa. These observations lead us to suggest that under normal physiological conditions, where I-mfa is quickly down-regulated by RANKL while TRPC1ϵ is up-regulated, TRPC1 can promote osteoclastogenesis. In regard to the genetic interaction of *Trpc1* and *I-mfa* in osteoclastogenesis, we propose that maximal and/or persistent activation of I_{CRAC}/I_{SOC} through TRPC1 in cells lacking I-mfa leads to excessive osteoclastogenesis and reduced bone mass. This suggestion is supported by our experiments in myeloid precursors and in studies in *Orai1* null mice showing similar but more severely defective osteoclastogenesis (51) and *in vitro* studies using Orai1-depleted osteoclasts (52, 53). The more severe and nonspecific effect of the deletion of *Orai1* in numerous cell types, including osteoclasts compared with TRPC1, is in agreement with Orai1 being a core component of the CRAC channel and TRPC1 being a regulatory protein whose function is dispensable for Orai1.

The TRPC1/I-mfa interaction is likely to affect osteoclastogenesis at both an early stage, possibly at a step sensitive to M-CSF-induced Ca^{2+} signaling and at a later stage affecting bone resorption. The idea that an early step is affected by TRPC1 and I-mfa is supported by the M-CSF-induced expression of *I-mfa* and *Trpc1*ϵ mRNAs in myeloid precursors, promoting not only the formation of a highly Ca^{2+}-selective CRAC channel complex but also its negative regulation by I-mfa. Our electrophysiological experiments in these cells clearly demonstrate a role of these two proteins in Ca^{2+} signaling at this stage of osteoclastogenesis. However, we cannot pinpoint which TRPC1 isoform is responsible for the observed effects on Ca^{2+} signaling and phenotypes associated with osteoclastogenesis. The development of a linear current in cells lacking I-mfa clearly argues for the functional expression of TRPC1α in these cells. However, a role of TRPC1ϵ cannot be ruled out, as the contribution of TRPC1α, TRPC1ϵ, or other TRPC1 isoforms in the inward component of store operated currents in these cells is unknown.

In regard to the molecular mechanism by which *Trpc1* and *I-mfa* affect early osteoclastogenesis, we speculate that M-CSF "primes" myeloid precursors for RANKL-mediated signaling, not only through the well known up-regulation of RANK (54) but also through the up-regulation of both TRPC1ϵ and I-mfa (Fig. 11). However, Ca^{2+} signaling and downstream activation of NFATc1 is suppressed at this stage as I-mfa suppresses CRAC channel activity through TRPC1ϵ. Upon stimulation with RANKL, cells become competent for Ca^{2+} signaling by down-regulating I-mfa releasing the block on CRAC channel. This idea is consistent with the lack of an effect of I-mfa on a specific class of osteoclasts (small, medium, or large sized), as all groups were up-regulated proportionally, arguing against a possible effect of I-mfa within the differentiation process. One possibility is that I-mfa suppresses the survival and/or proliferation of early osteoclast progenitors in response to M-CSF. Interestingly, M-CSF signaling is essential for the proliferation and survival of these progenitors through the up-regulation of β-catenin mediated by the action of the Ca^{2+}-sensitive Pyk2 tyrosine kinase (3). Therefore, we could envision a positive feedback loop whereby accumulated β-catenin could compete with TRPC1 for binding to I-mfa, relieving the I-mfa-mediated suppression of TRPC1 activity, thus allowing for Ca^{2+} influx. A recent study showed that M-CSF instructs hematopoietic stem cells toward the myeloid lineage in addition to previously known effects on survival and/or proliferation of committed hematopoietic progenitors (55). In light of these data, our study

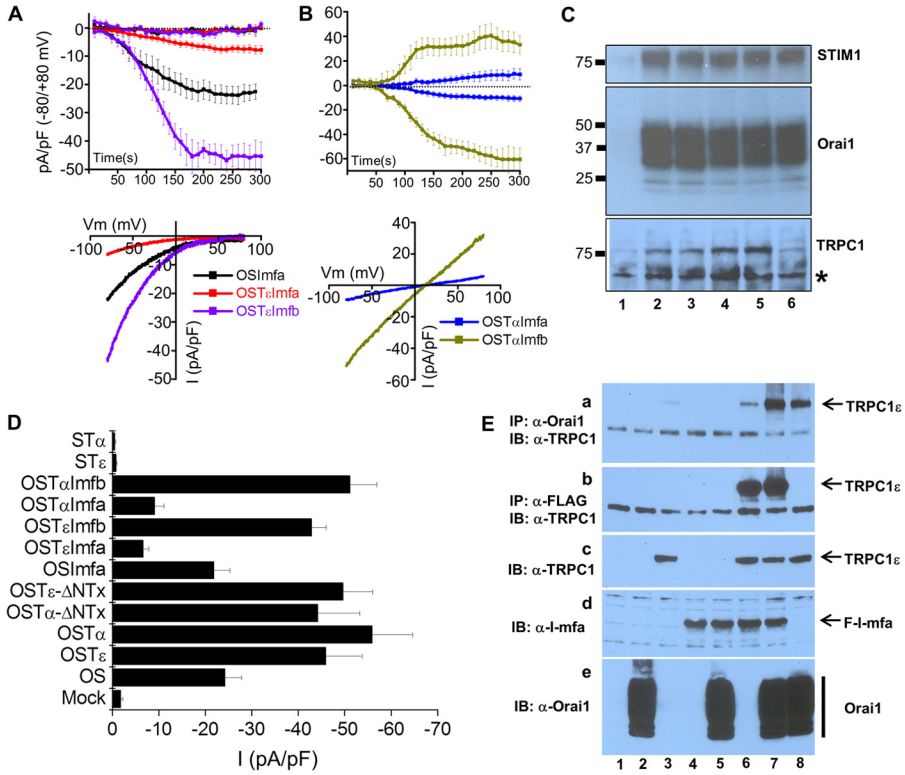

FIGURE 10. **Suppression of I_{CRAC} and I_{SOC} by I-mfa.** *A,* time course and *I–V* curves (taken at 200 s) of BAPTA-induced whole cell currents in HEK293 cells transfected with STIM1 (1.6 μg), Orai1 (1 μg), and I-mfa (0.3 μg) (*OSImfa, black, n* = 7), STIM1 (1.6 μg), Orai1 (1 μg), TRPC1ϵ (1 μg), and I-mfa (0.3 μg) (*OSTεImfa, red, n* = 10), or STIM1 (1.6 μg), Orai1 (1 μg), TRPC1ϵ (1 μg), and I-mfb (0.3 μg) (*OSTεImfb, violet, n* = 8). *B,* time course and *I–V* curves (taken at 200 s) of BAPTA-induced whole cell currents in HEK293 cells transfected with STIM1 (1.6 μg), Orai1 (1 μg), TRPC1α (1 μg), and I-mfa (0.3 μg) (*OSTαImfa, blue, n* = 10), or STIM1 (1.6 μg), Orai1 (1 μg), TRPC1α (1 μg), and I-mfb (0.3 μg) (*OSTαImfb, green, n* = 8). *C,* expression levels of Orai1, STIM1, TRPC1ϵ, and TRPC1α in HEK293 cell lysates transfected with pCDNA3 (*lane 1*), Orai1, STIM1, TRPC1ϵ, and FLAG-tagged I-mfa (*lane 2*), Orai1, STIM1, TRPC1ϵ, HA-tagged I-mfb (*lane 3*), Orai1, STIM1, TRPC1α, and FLAG-tagged I-mfa (*lane 4*), Orai1, STIM1, TRPC1α, and HA-tagged I-mfb (*lane 5*), or Orai1, STIM1, and FLAG-tagged I-mfa (*lane 6*). *Asterisk* indicates a nonspecific band. *D,* summary data showing the effect of indicated plasmids on BAPTA-induced I_{CRAC} or I_{SOC} density at −80 mV obtained 200 s following break-in in HEK293 cells. *pF,* picofarad. *E,* I-mfa does not disrupt the association of Orai1 and TRPC1. *Panel a,* HEK293T cells were transfected with pCDNA3 (mock, *lane 1*), Orai1 (*lane 2*), TRPC1ϵ (*lane 3*), FLAG-tagged I-mfa (*F-I-mfa*, *lane 4*), Orai1 + F-I-mfa (*lane 5*), F-I-mfa and TRPC1ϵ (*lane 6*), Orai1 + F-I-mfa + TRPC1ϵ (*lane 7*), or Orai1 + TRPC1ϵ (*lane 8*). Endogenous and transfected Orai1 was immunoprecipitated (*IP*) with α-Orai1, and association with transfected TRPC1ϵ was determined by immunoblotting (*IB*) using α-TRPC1. *Panel b,* association of F-Imfa and TRPC1 was determined by immunoprecipitation with α-FLAG and immunoblotting using α-TRPC1. *Panels c–e,* input amounts of TRPC1ϵ, F-I-mfa, or Orai1.

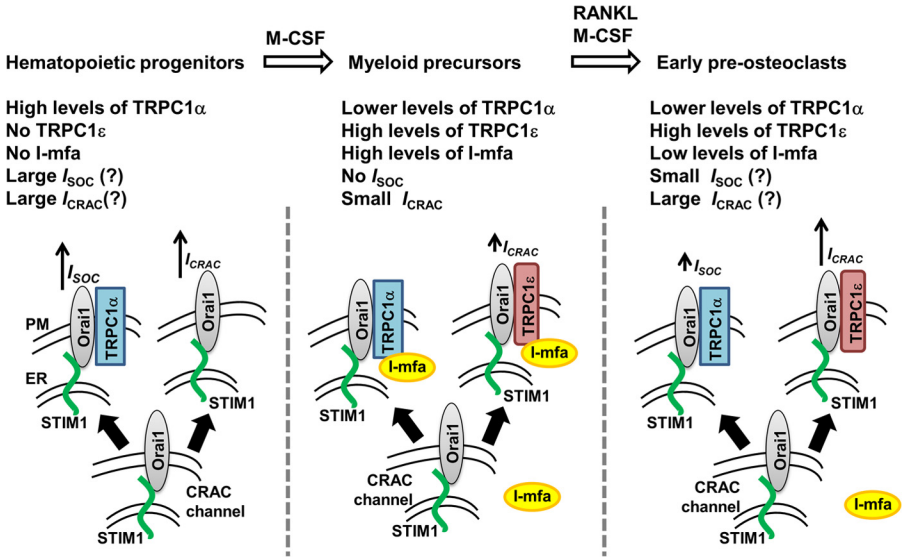

FIGURE 11. **Hypothetical model for the modulation of I_{SOC} and I_{CRAC} by TRPC1 and I-mfa in early stages of osteoclastogenesis.** M-CSF primes myeloid precursors for Ca^{2+} signaling by up-regulating not only TRPC1ϵ but also its negative regulator, I-mfa. As a result, Ca^{2+} signaling is maintained at a low level in this stage. In response to RANKL, I-mfa is down-regulated, although TRPC1ϵ expression persists, setting up myeloid precursors/early pre-osteoclasts highly competent for Ca^{2+} signaling, which is crucial for the downstream activation of NFATc1 and other regulators of osteoclastogenesis.

has implications in M-CSF-induced differentiation of hematopoietic stem cells. Future studies are needed to investigate which M-CSF-dependent process is affected by TRPC1/I-mfa-mediated Ca^{2+} signaling.

The enhanced ability of I-mfa-deficient osteoclasts to resorb bone is consistent with a role of TRPC1 in the regulation of secretion *per se* through SOCE channels. In fact, TRPC1 knockout mice used in our study show severely reduced salivary gland fluid secretion (56), and secretion and exocytosis are known functions of the CRAC channel (11). Therefore, it is tempting to speculate that increased resorptive activity in I-mfa-deficient osteoclasts is due to enhanced acid secretion secondary to up-regulated SOCE.

We present several lines of evidence supporting the hypothesis that Orai1 forms a complex with TRPC1. First, the TRPC1α and TRPC1ϵ isoforms require Orai1 for functional expression. Second, transfected TRPC1 co-immunoprecipitates with endogenous or transfected Orai1 in HEK293T cells. Third, TRPC1α and TRPC1ϵ each modulate the current mediated by Orai1, by generating I_{SOC} or by forming a Ba^{2+}-permeable channel complex, respectively. Fourth, I-mfa suppresses Orai1-mediated current only in the presence of TRPC1ϵ. These data lead us to propose a model whereby STIM1 and Orai1 form the core module of the CRAC channel, whereas TRPC1 and I-mfa form a regulatory module that enhances the dynamic range of this channel. However, we do not completely understand how this channel complex is formed. One possibility is that TRPC1α/ϵ and Orai1 form a heteromultimeric complex with a "chimeric" pore region. A second possibility is that they form different assemblies, but TRPC1 can regulate the activity of Orai1 by physical interactions through cytosolic fragments, possibly interfering with the gating of Orai1 by STIM1. We favor the second possibility, for several reasons. First, it is difficult to envision how TRPC1α/Orai1 and TRPC1ϵ/Orai1 could have different chimeric pores, because TRPC1α and TRPC1ϵ only differ by seven amino acids, which are located in N-terminal cytosolic region of TRPC1α. Second, the crystal structure of Orai1 revealed that purified Orai1 could form a functional pore without the need for additional subunits (57). Third, STIM1 not only gates but also determines the cation selectivity of Orai1 (50, 58). Therefore, it is conceivable that physical interactions through the N-terminal cytosolic region of TRPC1 and Orai1 could indirectly affect the cation permeability of Orai1 by interfering with binding to STIM1. We also favor this model because it does not require TRPC1 and Orai1 to be present in the same membrane. For example, TRPC1 can be in the endoplasmic reticulum or the plasma membrane.

The formation of I_{SOC} or I_{CRAC} by different TRPC1 isoforms implies that the magnitude of I_{CRAC} and I_{SOC} in different cell types can greatly vary depending on the expression levels of TRPC1 and I-mfa, even if levels of STIM1 and Orai1 are similar. Furthermore, our model implies that a cell would express I_{SOC} or I_{CRAC} depending on the TRPC1 isoform present in the cell. If there is no TRPC1 expression or I-mfa is in excess of TRPC1, cells would have Orai(1–3)-mediated I_{CRAC}. TRPC1 isoform switching in response to an extracellular stimulus (*i.e.* M-CSF in osteoclast precursors) along with the profound functional differences between isoforms adds an additional layer of complexity in the regulation of SOCE channels.

Our studies suggest that modulating the dynamic range of the CRAC channel can control osteoclastogenesis. Therefore, inhibition of TRPC1 through small molecules or pore-blocking antibodies, suppression of its expression, or up-regulation of I-mfa could constitute new ways to combat conditions associated with abnormally enhanced osteoclastogenesis. Many disease states, including chronic periodontitis, osteoporosis, rheumatoid arthritis, Paget disease, and cancer metastases develop when osteoclasts are excessively recruited or inappropriately activated. Targeting TRPC1 in these conditions can be considered more advantageous than targeting STIM and/or Orai molecules, which can have more severe and widespread side effects. Alternatively, small molecule inhibitors targeting the interaction between TRPC1 and I-mfa might be beneficial for high bone mass-related diseases such as osteopetrosis, where the balance is shifted toward reduced osteoclastogenesis. Although it is premature to speculate on targeting strategies at this time, our work offers new approaches to therapeutic interventions for a wide variety of bone diseases.

Acknowledgments—We thank Drs. Reinhold Penner, Jim Putney, Patrick Delmas, Gerard Elberg, and Ralf Janknecht for comments on the manuscript; Stephen Tapscott and Lauren Snider for I-mfa$^{+/-}$ mice, and the University of Alabama at Birmingham Center for Metabolic Bone Disease for histology and histomorphometric analysis.

REFERENCES

1. Hamilton, J. A. (2008) Colony-stimulating factors in inflammation and autoimmunity. *Nat. Rev. Immunol.* **8,** 533–544
2. Kong, Y. Y., Yoshida, H., Sarosi, I., Tan, H. L., Timms, E., Capparelli, C., Morony, S., Oliveira-dos-Santos, A. J., Van, G., Itie, A., Khoo, W., Wakeham, A., Dunstan, C. R., Lacey, D. L., Mak, T. W., Boyle, W. J., and Penninger, J. M. (1999) OPGL is a key regulator of osteoclastogenesis, lymphocyte development, and lymph-node organogenesis. *Nature* **397,** 315–323
3. Otero, K., Turnbull, I. R., Poliani, P. L., Vermi, W., Cerutti, E., Aoshi, T., Tassi, I., Takai, T., Stanley, S. L., Miller, M., Shaw, A. S., and Colonna, M. (2009) Macrophage colony-stimulating factor induces the proliferation and survival of macrophages via a pathway involving DAP12 and β-catenin. *Nat. Immunol.* **10,** 734–743
4. Takayanagi, H., Kim, S., Koga, T., Nishina, H., Isshiki, M., Yoshida, H., Saiura, A., Isobe, M., Yokochi, T., Inoue, J., Wagner, E. F., Mak, T. W., Kodama, T., and Taniguchi, T. (2002) Induction and activation of the transcription factor NFATc1 (NFAT2) integrate RANKL signaling in terminal differentiation of osteoclasts. *Dev. Cell* **3,** 889–901
5. Negishi-Koga, T., and Takayanagi, H. (2009) Ca^{2+}-NFATc1 signaling is an essential axis of osteoclast differentiation. *Immunol. Rev.* **231,** 241–256
6. Masuyama, R., Vriens, J., Voets, T., Karashima, Y., Owsianik, G., Vennekens, R., Lieben, L., Torrekens, S., Moermans, K., Vanden Bosch, A., Bouillon, R., Nilius, B., and Carmeliet, G. (2008) TRPV4-mediated calcium influx regulates terminal differentiation of osteoclasts. *Cell Metab.* **8,** 257–265
7. van der Eerden, B. C., Hoenderop, J. G., de Vries, T. J., Schoenmaker, T., Buurman, C. J., Uitterlinden, A. G., Pols, H. A., Bindels, R. J., and van Leeuwen, J. P. (2005) The epithelial Ca^{2+} channel TRPV5 is essential for proper osteoclastic bone resorption. *Proc. Natl. Acad. Sci. U.S.A.* **102,** 17507–17512
8. Kajiya, H., Okamoto, F., Nemoto, T., Kimachi, K., Toh-Goto, K., Nakayana, S., and Okabe, K. (2010) RANKL-induced TRPV2 expression regulates osteoclastogenesis via calcium oscillations. *Cell Calcium* **48,**

260–269
9. Hoth, M., and Penner, R. (1992) Depletion of intracellular calcium stores activates a calcium current in mast cells. *Nature* **355,** 353–356
10. Birnbaumer, L. (2009) The TRPC class of ion channels: a critical review of their roles in slow, sustained increases in intracellular Ca^{2+} concentrations. *Annu. Rev. Pharmacol. Toxicol.* **49,** 395–426
11. Parekh, A. B., and Putney, J. W., Jr. (2005) Store-operated calcium channels. *Physiol. Rev.* **85,** 757–810
12. Zhang, S. L., Yeromin, A. V., Zhang, X. H., Yu, Y., Safrina, O., Penna, A., Roos, J., Stauderman, K. A., and Cahalan, M. D. (2006) Genome-wide RNAi screen of Ca^{2+} influx identifies genes that regulate Ca^{2+} release-activated Ca^{2+} channel activity. *Proc. Natl. Acad. Sci. U.S.A.* **103,** 9357–9362
13. Peinelt, C., Vig, M., Koomoa, D. L., Beck, A., Nadler, M. J., Koblan-Huberson, M., Lis, A., Fleig, A., Penner, R., and Kinet, J. P. (2006) Amplification of CRAC current by STIM1 and CRACM1 (Orai1). *Nat. Cell Biol.* **8,** 771–773
14. Soboloff, J., Spassova, M. A., Tang, X. D., Hewavitharana, T., Xu, W., and Gill, D. L. (2006) Orai1 and STIM reconstitute store-operated calcium channel function. *J. Biol. Chem.* **281,** 20661–20665
15. Mercer, J. C., Dehaven, W. I., Smyth, J. T., Wedel, B., Boyles, R. R., Bird, G. S., and Putney, J. W., Jr. (2006) Large store-operated calcium selective currents due to co-expression of Orai1 or Orai2 with the intracellular calcium sensor, Stim1. *J. Biol. Chem.* **281,** 24979–24990
16. Prakriya, M., Feske, S., Gwack, Y., Srikanth, S., Rao, A., and Hogan, P. G. (2006) Orai1 is an essential pore subunit of the CRAC channel. *Nature* **443,** 230–233
17. Feske, S., Gwack, Y., Prakriya, M., Srikanth, S., Puppel, S. H., Tanasa, B., Hogan, P. G., Lewis, R. S., Daly, M., and Rao, A. (2006) A mutation in Orai1 causes immune deficiency by abrogating CRAC channel function. *Nature* **441,** 179–185
18. Wang, Y., Deng, X., Zhou, Y., Hendron, E., Mancarella, S., Ritchie, M. F., Tang, X. D., Baba, Y., Kurosaki, T., Mori, Y., Soboloff, J., and Gill, D. L. (2009) STIM protein coupling in the activation of Orai channels. *Proc. Natl. Acad. Sci. U.S.A.* **106,** 7391–7396
19. Vig, M., Peinelt, C., Beck, A., Koomoa, D. L., Rabah, D., Koblan-Huberson, M., Kraft, S., Turner, H., Fleig, A., Penner, R., and Kinet, J. P. (2006) CRACM1 is a plasma membrane protein essential for store-operated Ca^{2+} entry. *Science* **312,** 1220–1223
20. Liou, J., Kim, M. L., Heo, W. D., Jones, J. T., Myers, J. W., Ferrell, J. E., Jr., and Meyer, T. (2005) STIM is a Ca^{2+} sensor essential for Ca^{2+}-store depletion-triggered Ca^{2+} influx. *Curr. Biol.* **15,** 1235–1241
21. Brandman, O., Liou, J., Park, W. S., and Meyer, T. (2007) STIM2 is a feedback regulator that stabilizes basal cytosolic and endoplasmic reticulum Ca^{2+} levels. *Cell* **131,** 1327–1339
22. Roos, J., DiGregorio, P. J., Yeromin, A. V., Ohlsen, K., Lioudyno, M., Zhang, S., Safrina, O., Kozak, J. A., Wagner, S. L., Cahalan, M. D., Veliçelebi, G., and Stauderman, K. A. (2005) STIM1, an essential and conserved component of store-operated Ca^{2+} channel function. *J. Cell Biol.* **169,** 435–445
23. Zhang, S. L., Yu, Y., Roos, J., Kozak, J. A., Deerinck, T. J., Ellisman, M. H., Stauderman, K. A., and Cahalan, M. D. (2005) STIM1 is a Ca^{2+} sensor that activates CRAC channels and migrates from the Ca^{2+} store to the plasma membrane. *Nature* **437,** 902–905
24. Luik, R. M., Wu, M. M., Buchanan, J., and Lewis, R. S. (2006) The elementary unit of store-operated Ca^{2+} entry: local activation of CRAC channels by STIM1 at ER-plasma membrane junctions. *J. Cell Biol.* **174,** 815–825
25. Wu, M. M., Buchanan, J., Luik, R. M., and Lewis, R. S. (2006) Ca^{2+} store depletion causes STIM1 to accumulate in ER regions closely associated with the plasma membrane. *J. Cell Biol.* **174,** 803–813
26. Muik, M., Fahrner, M., Schindl, R., Stathopulos, P., Frischauf, I., Derler, I., Plenk, P., Lackner, B., Groschner, K., Ikura, M., and Romanin, C. (2011) STIM1 couples to ORAI1 via an intramolecular transition into an extended conformation. *EMBO J.* **30,** 1678–1689
27. Stathopulos, P. B., Zheng, L., Li, G. Y., Plevin, M. J., and Ikura, M. (2008) Structural and mechanistic insights into STIM1-mediated initiation of store-operated calcium entry. *Cell* **135,** 110–122
28. Vig, M., Beck, A., Billingsley, J. M., Lis, A., Parvez, S., Peinelt, C., Koomoa, D. L., Soboloff, J., Gill, D. L., Fleig, A., Kinet, J. P., and Penner, R. (2006) CRACM1 multimers form the ion-selective pore of the CRAC channel. *Curr. Biol.* **16,** 2073–2079
29. Yeromin, A. V., Zhang, S. L., Jiang, W., Yu, Y., Safrina, O., and Cahalan, M. D. (2006) Molecular identification of the CRAC channel by altered ion selectivity in a mutant of Orai. *Nature* **443,** 226–229
30. Yuan, J. P., Zeng, W., Huang, G. N., Worley, P. F., and Muallem, S. (2007) STIM1 heteromultimerizes TRPC channels to determine their function as store-operated channels. *Nat. Cell Biol.* **9,** 636–645
31. Huang, G. N., Zeng, W., Kim, J. Y., Yuan, J. P., Han, L., Muallem, S., and Worley, P. F. (2006) STIM1 carboxyl-terminus activates native SOC, I_{crac}, and TRPC1 channels. *Nat. Cell Biol.* **8,** 1003–1010
32. Singh, B. B., Liu, X., Tang, J., Zhu, M. X., and Ambudkar, I. S. (2002) Calmodulin regulates Ca^{2+}-dependent feedback inhibition of store-operated Ca^{2+} influx by interaction with a site in the C terminus of TrpC1. *Mol. Cell* **9,** 739–750
33. Cheng, K. T., Liu, X., Ong, H. L., Swaim, W., and Ambudkar, I. S. (2011) Local Ca^{2+} entry via Orai1 regulates plasma membrane recruitment of TRPC1 and controls cytosolic Ca^{2+} signals required for specific cell functions. *PLoS Biol.* **9,** e1001025
34. Wang, Y., Deng, X., Mancarella, S., Hendron, E., Eguchi, S., Soboloff, J., Tang, X. D., and Gill, D. L. (2010) The calcium store sensor, STIM1, reciprocally controls Orai and CaV1.2 channels. *Science* **330,** 105–109
35. Cheng, K. T., Liu, X., Ong, H. L., and Ambudkar, I. S. (2008) Functional requirement for Orai1 in store-operated TRPC1-STIM1 channels. *J. Biol. Chem.* **283,** 12935–12940
36. Liao, Y., Erxleben, C., Abramowitz, J., Flockerzi, V., Zhu, M. X., Armstrong, D. L., and Birnbaumer, L. (2008) Functional interactions among Orai1, TRPCs, and STIM1 suggest a STIM-regulated heteromeric Orai/TRPC model for SOCE/Icrac channels. *Proc. Natl. Acad. Sci. U.S.A.* **105,** 2895–2900
37. Liao, Y., Erxleben, C., Yildirim, E., Abramowitz, J., Armstrong, D. L., and Birnbaumer, L. (2007) Orai proteins interact with TRPC channels and confer responsiveness to store depletion. *Proc. Natl. Acad. Sci. U.S.A.* **104,** 4682–4687
38. Shi, J., Ju, M., Abramowitz, J., Large, W. A., Birnbaumer, L., and Albert, A. P. (2012) TRPC1 proteins confer PKC and phosphoinositol activation on native heteromeric TRPC1/C5 channels in vascular smooth muscle: comparative study of wild-type and $TRPC1^{-/-}$ mice. *FASEB J.* **26,** 409–419
39. Chen, C. M., Kraut, N., Groudine, M., and Weintraub, H. (1996) I-mf, a novel myogenic repressor, interacts with members of the MyoD family. *Cell* **86,** 731–741
40. Snider, L., Thirlwell, H., Miller, J. R., Moon, R. T., Groudine, M., and Tapscott, S. J. (2001) Inhibition of Tcf3 binding by I-mfa domain proteins. *Mol. Cell. Biol.* **21,** 1866–1873
41. Snider, L., and Tapscott, S. J. (2005) XIC is required for Siamois activity and dorsoanterior development. *Mol. Cell. Biol.* **25,** 5061–5072
42. Pan, W., Jia, Y., Wang, J., Tao, D., Gan, X., Tsiokas, L., Jing, N., Wu, D., and Li, L. (2005) β-Catenin regulates myogenesis by relieving I-mfa-mediated suppression of myogenic regulatory factors in P19 cells. *Proc. Natl. Acad. Sci. U.S.A.* **102,** 17378–17383
43. Kusano, S., and Raab-Traub, N. (2002) I-mfa domain proteins interact with axin and affect its regulation of the Wnt and c-Jun N-terminal kinase signaling pathways. *Mol. Cell. Biol.* **22,** 6393–6405
44. Ma, R., Rundle, D., Jacks, J., Koch, M., Downs, T., and Tsiokas, L. (2003) Inhibitor of myogenic family, a novel suppressor of store-operated currents through an interaction with TRPC1. *J. Biol. Chem.* **278,** 52763–52772
45. Kraut, N., Snider, L., Chen, C. M., Tapscott, S. J., and Groudine, M. (1998) Requirement of the mouse I-mfa gene for placental development and skeletal patterning. *EMBO J.* **17,** 6276–6288
46. Dietrich, A., Kalwa, H., Storch, U., Mederos, y, Schnitzler, M., Salanova, B., Pinkenburg, O., Dubrovska, G., Essin, K., Gollasch, M., Birnbaumer, L., and Gudermann, T. (2007) Pressure-induced and store-operated cation influx in vascular smooth muscle cells is independent of TRPC1. *Pflugers Arch.* **455,** 465–477
47. Parfitt, A. M., Drezner, M. K., Glorieux, F. H., Kanis, J. A., Malluche, H.,

Meunier, P. J., Ott, S. M., and Recker, R. R. (1987) Bone histomorphometry: standardization of nomenclature, symbols, and units. Report of the ASBMR histomorphometry nomenclature committee. *J. Bone Miner. Res.* **2,** 595–610
48. Sakura, H., and Ashcroft, F. M. (1997) Identification of four *trp1* gene variants murine pancreatic beta-cells. *Diabetologia* **40,** 528–532
49. Ivanov, I. P., Firth, A. E., Michel, A. M., Atkins, J. F., and Baranov, P. V. (2011) Identification of evolutionarily conserved non-AUG-initiated N-terminal extensions in human coding sequences. *Nucleic Acids Res.* **39,** 4220–4234
50. Scrimgeour, N., Litjens, T., Ma, L., Barritt, G. J., and Rychkov, G. Y. (2009) Properties of Orai1 mediated store-operated current depend on the expression levels of STIM1 and Orai1 proteins. *J. Physiol.* **587,** 2903–2918
51. Robinson, L. J., Mancarella, S., Songsawad, D., Tourkova, I. L., Barnett, J. B., Gill, D. L., Soboloff, J., and Blair, H. C. (2012) Gene disruption of the calcium channel Orai1 results in inhibition of osteoclast and osteoblast differentiation and impairs skeletal development. *Lab. Invest.* **92,** 1071–1083
52. Hwang, S. Y., and Putney, J. W. (2012) Orai1-mediated calcium entry plays a critical role in osteoclast differentiation and function by regulating activation of the transcription factor NFATc1. *FASEB J.* **26,** 1484–1492
53. Zhou, Y., Lewis, T. L., Robinson, L. J., Brundage, K. M., Schafer, R., Martin, K. H., Blair, H. C., Soboloff, J., and Barnett, J. B. (2011) The role of calcium release activated calcium channels in osteoclast differentiation. *J. Cell. Physiol.* **226,** 1082–1089
54. Arai, F., Miyamoto, T., Ohneda, O., Inada, T., Sudo, T., Brasel, K., Miyata, T., Anderson, D. M., and Suda, T. (1999) Commitment and differentiation of osteoclast precursor cells by the sequential expression of c-Fms and receptor activator of nuclear factor κB (RANK) receptors. *J. Exp. Med.* **190,** 1741–1754
55. Mossadegh-Keller, N., Sarrazin, S., Kandalla, P. K., Espinosa, L., Stanley, E. R., Nutt, S. L., Moore, J., and Sieweke, M. H. (2013) M-CSF instructs myeloid lineage fate in single haematopoietic stem cells. *Nature* **497,** 239–243
56. Liu, X., Cheng, K. T., Bandyopadhyay, B. C., Pani, B., Dietrich, A., Paria, B. C., Swaim, W. D., Beech, D., Yildrim, E., Singh, B. B., Birnbaumer, L., and Ambudkar, I. S. (2007) Attenuation of store-operated Ca^{2+} current impairs salivary gland fluid secretion in TRPC1(−/−) mice. *Proc. Natl. Acad. Sci. U.S.A.* **104,** 17542–17547
57. Hou, X., Pedi, L., Diver, M. M., and Long, S. B. (2012) Crystal structure of the calcium release-activated calcium channel Orai. *Science* **338,** 1308–1313
58. McNally, B. A., Somasundaram, A., Yamashita, M., and Prakriya, M. (2012) Gated regulation of CRAC channel ion selectivity by STIM1. *Nature* **482,** 241–245